# Expansion of mammary intraepithelial lymphocytes and intestinal inputs shape T cell dynamics in lactogenesis.

*Abigail Jaquish[1,2], Eleni Phung[1], Xutong Gong[3], Pilar Baldominos[4], Silvia Galvan-Pena[3], Isabelle Bursulaya[1], Ian Magill[3], Eleonara Marina[4], ImmgenT consortium*, Kerri Bertrand[5], Christina Chambers[5], Andrés R. Muñoz-Rojas[6], Judith Agudo[3,5,7,8], Diane Mathis[3], Christophe Benoist[3], Deepshika Ramanan[1,3].*

[1]NOMIS Center for Immunobiology and Microbial Pathogenesis, Salk Institute for Biological Studies, La Jolla, CA 92037, USA.

[2]Biological Sciences Graduate Program, University of California, San Diego, La Jolla, CA 92092, USA.

[3]Department of Immunology, Harvard Medical School, Boston, MA 02115, USA.

[4]Department of Cancer Immunology and Virology, Dana-Farber Cancer Institute, Boston, MA 02215, USA.

[5]Department of Pediatrics, University of California, San Diego, La Jolla, CA 92093, USA.

[6]Department of Biomedical Engineering, Rensselaer Polytechnic Institute, Troy, NY 12180, USA

[7]Parker Institute for Cancer Immunotherapy at Dana-Farber Cancer Institute, Boston, MA 02215, USA.

[8]New York Stem Cell Foundation, Robertson Investigator.

* ImmgenT consortium members listed at back.

**ABSTRACT**

Pregnancy brings about profound changes in the mammary gland to prepare for lactation, yet immunocyte changes that accompany this rapid remodeling are incompletely understood. We comprehensively analyzed mammary T cells, revealing a marked increase in CD4+ and CD8+ T effector cells, including an expansion of TCRαβ+CD8αα+ cells, in pregnancy and lactation. T cells were localized in the mammary epithelium, resembling intraepithelial lymphocytes (IELs) typically found in mucosal tissues. Similarity to mucosal tissues was substantiated by demonstrating partial dependence on microbial cues, T cell migration from the intestine to the mammary gland in late pregnancy, and shared TCR clonotypes between intestinal and mammary tissues, including intriguing public TCR families. Putative counterparts of mammary IELs were found in human breast and milk. Mammary T cells are thus poised to manage the transition from a non-mucosal tissue to a mucosal barrier during lactogenesis.

## INTRODUCTION

The mammary gland is remarkable in its capacity to undergo multiple cycles of growth and regression during reproductive years. Mammary gland remodeling is largely driven by hormonal cues, resulting in stage specific tissue adaptations during puberty, pregnancy, lactation, and involution[1, 2, 3]. Pregnancy initiates proliferation of mammary epithelial cells and ductal branching to support lactogenesis, a crucial process that ensures successful production and transfer of breast milk, essential for offspring health[4, 5]. The transition of the mammary gland into a secretory organ for the duration of lactation involves dramatic restructuring of cell composition and tissue enlargement, and increases its exposure to the outside environment, including microbes on maternal skin and offspring's oral cavity, rendering it a temporary barrier tissue[6, 7]. The end of lactation triggers mammary involution, a reversal to its non-secretory state marked by extensive apoptosis and tissue shrinkage[8, 9]. The physiological stress that accompanies the rapid transformation of the mammary gland requires an extensive support network, including immunocytes, but the types of immunocytes involved and their functions in lactogenesis are unclear.

Innate and adaptive immunocytes are involved in immune regulation of the mammary gland at various developmental stages. Mast cells and eosinophils promote ductal branching during mammary gland development in puberty[10, 11]. Macrophages are required for mammary gland morphogenesis in puberty, alveologenesis in pregnancy, and tissue regression in involution[11, 12, 13, 14, 15, 16]. A specialized population of macrophages called ductal macrophages dominate the lactating mammary gland, and another subtype of macrophages, lactation-induced macrophages (liMacs), have been recently identified to support lactogenesis and milk production[12, 17]. B cells, specifically IgA- and IgG-producing plasma cells, are abundant in lactation and promote offspring health by shaping the antibody composition of milk. We and others have shown that IgA-producing plasma cells can migrate from the intestine to the mammary gland in a CCL28 dependent manner[18, 19, 20, 21, 22]. Despite recent advances, our comprehension of various immunocyte types and their collaborative roles in facilitating mammary remodeling and regulating milk composition remains limited.

T cells play a fundamental role in tissue homeostasis by promoting defense, tolerance, tissue repair, and regulating cell proliferation and death. CD4+ T cells have been described in the

79 mammary gland in puberty, and a subset of CD4+ regulatory T cells (Tregs) that express RORγ
80 increase during involution[23, 24]. In addition, CD4+ and CD8+ T cells are present in milk[25].
81 Mammary γδ+ T cells with innate-like properties increase during lactation, and lack of these γδ+
82 T cells can favor mammary oncogenesis[26]. During lactogenesis, several processes occur
83 simultaneously, including epithelial cell stress from rapid expansion and milk production, and
84 heightened exposure to the sudden increase in newly revealed self-antigens, which could create a
85 conundrum for T cell tolerance, highlighting the need for T cell assistance. Yet, there is a large gap
86 in our understanding of which T cell subsets are involved in lactogenesis, and how they contribute
87 to tissue specific adaptations in the mammary gland during gestation, lactation, and involution.

88 We set out to define immunocyte changes in lactogenesis and uncovered novel T cell
89 dynamics in the mammary gland. We provide a detailed overview of mammary intraepithelial T
90 cells, shaped by intestinal and microbial influences, that accompany the remodeling of the
91 mammary gland into a mucosal-like state during lactogenesis.

92

93 **RESULTS**

94 ***Lactation leads to increased T cell activation in the mammary gland.***

95 The size and composition of the mammary gland undergo substantial changes in preparation for
96 lactation, yet there remains a gap in our understanding of how immunocytes adapt to, and perhaps
97 facilitate, those transitions. We first quantified mammary immunocytes (CD45+) across
98 developmental stages by flow cytometry and found that gestation (G) initiated a rapid increase in
99 the total number of immunocytes, that was maintained in lactation (L), and involution (I) (Fig.
100 1A). To determine the expanding cell types and chart their adaptations, we performed a temporal
101 analysis of immunocytes across different stages in female C57BL/6 (B6) mice; profiling by single-
102 cell RNA sequencing (scRNAseq) mammary glands from nulliparous, gestation (day 17), early
103 lactation (day 3 postpartum), and involution (day 1 post-weaning) stages, multiplexed into the
104 same runs. A total of 60,060 immunocytes were captured across all lineages from 20 mice across
105 three independent runs, revealing increased representation of T cell populations (Fig. S1A-B).
106 Validation by flow cytometry confirmed the expansion of T cells, while the proportion of myeloid
107 cells, which dominated in the nulliparous, declined somewhat (while remaining the largest cell
108 populations, as previously described[12, 17, 24] )(Fig. 1B). Analysis of the scRNAseq data revealed

109 several myeloid cell populations, including the recently described lactation associated liMacs,
110 specifically during lactation[17] (Fig. S1B,C). While we did not observe shifts in B cell populations,
111 we identified CD103+ NK cells that were associated with lactation (Fig. S1A, D). To better
112 understand the expanding T cell populations, we applied Louvain clustering[27], which parsed 6
113 clusters of T cells, which were annotated as naïve T cells (Tn), and effector T cells (Teff) that were
114 either CD4+, CD8αβ+ or CD8α+CD8β- (CD8αα), and CD4-CD8-CD3+ (Double negative, DN)
115 (Fig. 1C, replicate in Fig. S2A) (gene signatures from ImmGen[28, 29, 30]). There was a strong shift
116 in the relative proportions of naïve vs activated states of CD4+ T cells and CD8+ T cells, from
117 mostly naïve T cells before and during gestation to mostly activated states during lactation, with a
118 particularly striking increase in CD8αα+ Teff in late pregnancy that persisted during involution
119 (Fig. 1C). This shift was observed among all TCRβ+ populations in the mammary gland by flow
120 cytometry (Fig. S2B).

121 In contrast to the CD8αβ+ Teff cells characterized by *Itgb1* and *Cxcr6* expression, CD8αα+ Teff
122 cells also expressed high levels of *Klrb1c*, *Cd160, Itgae*, and *Gzmb*, suggesting increased cytotoxic
123 potential and tissue residency (Fig. 1E, S3). CD8αα+ Teff cells also expressed increased cell
124 adhesion and proliferation genes such as *Mcm5, Mcm7, Mki67, Lgals1*, and *Hmmr* in differential
125 levels across stages (Fig. S2C-D, S3). The transcriptional signature of CD8αα+ cells was
126 reminiscent of CD8αα+ T cells[28, 30] that have innate properties and reside in the epithelium of
127 mucosal tissues, referred to as intraepithelial lymphocytes (IELs) (intestinal CD8αα+ IEL
128 signature[31,30,31] applied to mammary CD8αα+ cluster in Fig. 1C). A similar signature has also been
129 described in TCRαβ+ innate-like T cells with high cytotoxic potential in mammary tumors called
130 αβILTCKs[32] (Fig. S2E). CD8αα+ T cells mostly differentiate in the thymus in response to strong
131 agonists[32, 33, 34, 35, 36] and use either TCRαβ or TCRγδ, but mammary CD8αα+ T cells were mostly
132 TCRαβ+ (Fig. S4A). Flow cytometric validation confirmed that gestating and lactating mammary
133 glands displayed a significant increase in the proportion of CD8αα+ and DN T cells and in cell
134 numbers of CD4+ Teff, CD8+ Teff, and DN populations (denoted by CD44+ staining) (Fig. 1F-G,
135 gating strategy in S4B).

136 We investigated other T cell populations and interestingly, while Tregs increased during
137 gestation, lactation led to a significant drop in Treg proportions and numbers (Fig. S4C), followed

138 by an increase in involution. Unconventional T cell subsets such as γδ T cells, MR1+ MAIT cells
139 and iNKT cells were sparse, and to some extent, decreased upon lactation (Fig. S4D,E). Thus,
140 mammary gland remodeling is accompanied by strong changes in T cell populations, including a
141 hyper-activated state and increased CD4+ Teff, CD8αβ+ Teff, and CD8αα+ Teff cells in lactation,
142 presumably in response to rapid epithelial cell proliferation and exposure to the outside
143 environment.

144

145 ***Mammary T cell populations are located in the epithelium.***

146 The expansion of mammary CD8αα+ T cells, an abundant cell-type in the intestine, was intriguing.
147 To compare transcriptional similarities of CD8αα+ T cells across tissues, we multiplexed
148 nulliparous and lactating mammary gland, small and large intestine, and spleen from the same
149 mouse into scRNAseq experiments (Fig. 2A, 25,096 cells, 4 mice, 2 independent experiments). At
150 first glance T cells from the same tissue clustered together suggesting a distinct transcriptional
151 state that was tissue specific (Fig. 2A). However, signatures of effector CD4+, CD8αβ+, and
152 CD8αα+ T cells were similar across organs (Fig. 2B). Most CD8αα+ T cell genes, *Tyrobp*,
153 *Fcer1g*, *Itgae*, *Gzmb*, displayed similar expression in mammary gland, small intestine and large
154 intestine but not the spleen (Fig. S5A). The expression of killer cell lectin-like receptor (KLR)
155 family genes such as *Klra1, Klra7, Klrb1a,* and *Klrb1c*, were higher in mammary CD8αα+ T cells
156 compared to intestinal tissues (Fig. S5A). We validated two of the classical IEL markers used
157 above by flow cytometry, Ly49a (*Klra1*) – a killer cell lectin like receptor that binds MHC-I, and
158 CD103 (*Itgae*), an integrin that mediates cell adhesion and tissue retention by binding to e-cadherin
159 on epithelial cells. In line with the gene expression data above, lactation led to increased Ly49a
160 expression in CD103+ CD8αα+ T cells in the mammary gland and to a lesser extent in the small
161 intestine (Fig. 2C, S5B). Lactation also led to a decrease in CD103+ CD8αα+ T cells in the small
162 intestine but not the mammary gland (Fig. 2C-D, S5B). We also observed a lactation-mediated
163 increase in the expression of markers associated with intestinal IELs, such as CD160, CD38, and
164 2B4 (CD244)[37, 38, 39], on mammary CD8αα+ and CD8αβ+T cells (Fig. 2D, S5C). Based on the
165 gene signatures and surface expression profiles, we hypothesized that CD8αα+ T cells in the
166 mammary gland could be IELs. Since the defining characteristic of IELs is their residence in the
167 epithelial layer, we surveyed the physical location of the effector T cells in the mammary gland

168 tissue. Indeed, we observed CD8αα+ T cells adjacent to both basal and luminal epithelial cells
169 (basal epithelial cells by Krt14 and luminal epithelial cells by Krt8), in increased numbers during
170 gestation and early lactation (Fig. 2E and S5D). Surprisingly, CD4+ and CD8αβ+ T cells were
171 also intraepithelial in location (Fig. 2E and S5D). Overall, our results demonstrate that mammary
172 CD8αα+ T cells have marked phenotypic similarity to intestinal CD8αα+ IELs. Mammary CD4+
173 and CD8αβ+ T cell populations are also IELs, reminiscent of mucosal epithelium. The increase in
174 mammary IELs in lactation is indicative of a temporary mucosal state of the reconfigured
175 mammary gland.

176

177 ***Putative mammary T cell-epithelial cell interaction networks shift during lactation.***
178 Given the intraepithelial location of expanding mammary T cells during lactation, we investigated
179 the potential interaction pathways between mammary IELs and basal and luminal epithelial cells
180 in nulliparous and lactating mammary glands using CellChat[40] (25,506 cells, 4 mice per condition).
181 [CellChat uses a manually curated database (CellChatDB) of literature-supported ligand:receptor
182 signaling pathways, including multisubunit structures, cofactors, coreceptors, agonists and
183 antagonists. Each potential interaction is assigned an interaction probability score based on the law
184 of mass action to model the likelihood of an interaction based on the expression of the ligand,
185 receptor, and any cofactors. Statistically significant interactions are identified through a
186 permutation test on randomly assigned group labels for cells]. We first identified differentially
187 expressed genes ($p < 0.05$) between nulliparous and lactating mice for each cell population, and
188 then mapped their projected interactions based on the fold change of ligands and receptors. For
189 visualization purposes, we combined ligand:receptor pairs into functionally related signaling
190 pathways (Fig. 3A,D, S6A,C), and plotted communication probabilities between ligand:receptor
191 pairs upregulated (Fig. 3B, S7) or downregulated (Fig. S6B,D) with lactation. Potential
192 interactions that were upregulated with lactation were enriched in pathways related to cell adhesion
193 and migration, including *Pecam1,* selectins (*Sell)*, laminins (*Lamb3*), and galectins (*Lgals9*) (Fig.
194 3A,B). Expression of *Lgals9* and *Lamb3* transcripts was increased in CD8αα+ and CD8αβ+ T
195 cells, while *Pecam1* and *Sell* expression was increased in CD4+ Teff cells and DN T cells (Fig
196 3C). Interestingly, *Sell* was highly expressed in nulliparous CD8αβ+ Teff cells, but its potential
197 interacting partner shifted from *Podxl* in nulliparous mice to *Glycam1* in lactation (Fig. 3B, S6B).

198 *Glycam1* is a mucin-like glycoprotein produced by luminal cells in a prolactin-dependent
199 manner[41], and could potentially facilitate epithelial-IEL interactions during lactogenesis.
200 Predicted interactions from epithelial cells to T cells were enriched for immunoregulatory
201 pathways in lactation, including increased expression of MHC complexes in basal epithelial cells
202 with MHC I signaling to CD8αα+ and CD8aβ+ IELs, and MHC II signaling to CD4+ Teff cells
203 (Fig. 3D,E, S7). Another strongly predicted interaction between luminal cells and multiple IEL
204 populations involves osteopontin (*Spp1*), a glycoprotein associated with epithelial cell
205 proliferation and local immunity during lactation[42] (Fig. 3D,E and S7). Thus, putative interaction
206 analysis suggests multiple signaling pathways between epithelial cells and intraepithelial T cells
207 which could regulate immune surveillance and lactogenesis, providing candidates for future
208 functional studies.

209

210 ***T cells migrate from the intestine during gestation.***

211 Intestinal TCRαβ+ CD8αα+ IELs arise from thymic progenitors acquiring their effector
212 program and expression of gut-homing receptors in the thymus as a result of agonist stimulation
213 by self-antigens [32, 33, 34, 35, 36]. To test whether the strong increase in mammary gland CD8αα+ IELs
214 stemmed directly from the thymus, we thymectomized female mice before pregnancy (4 weeks of
215 age) and assessed mammary gland CD8αα+ IELs during lactation. Surprisingly, there were no
216 differences between thymectomized and control mice in numbers of CD8αα+ IELs or other T cell
217 subsets in the lactating mammary gland (Fig. 4A). There were also no differences in previously
218 described thymic progenitor subsets (PD-1+ or T-bet+) [43] in the lactating thymus when compared
219 to nulliparous mice (Fig. S8A). This raises two possibilities: either thymic progenitors seed the
220 mammary gland before 4 weeks of age and these few T cells expand into CD8αα+ IELs during
221 pregnancy, or mammary CD8αα+ IELs are of extrathymic origin, potentially from other mucosal
222 sites, and migrate to the mammary gland during late pregnancy. We found a modest increase in
223 Ki67+ T cells during gestation, but not lactation, suggesting that the expansion of mammary T
224 cells could be a combination of proliferation of mammary T cells and extrathymic input (Fig. S8B).
225 We previously used Kaede photoconvertible mice to track the migration of immunocytes from the
226 intestines to other body locations[44]. Among migratory intestinal cells in the spleen was a small

227 population of IEL-like CD8αα+ TCRαβ+ cells, which led us to hypothesize that mammary
228 CD8αα+ IELs could be of intestinal origin[44]. To test this hypothesis, intestinal sections (small
229 intestine, excluding Peyer's patches) of Kaede mice were photoconverted from green to red, at
230 different times of gestation and early lactation, and mammary glands were analyzed 24hrs later
231 (Fig. 4B). Importantly, due to the challenges associated with performing surgery in pregnant mice,
232 only a small fraction of the intestine, accessible with minimal disturbance to surrounding tissues,
233 was photoconverted. Kaede-red cells of intestinal origin had indeed migrated to the mammary
234 gland, including all three CD8αα+, CD4+ and CD8αβ+ T cell types (Fig. 4C), and to the spleen
235 as previously reported[44] (Fig S8C). Although from small numbers, this observation indicates that
236 some intestinal T cells migrated to the mammary gland within this one-day period. Thus, expansion
237 of mammary T cells in late pregnancy and lactation is driven by thymic and intestinal inputs.

238

239 ***T cell clones are shared between intestinal IELs and mammary IELs.***

240 To further establish the relationship between intestinal and mammary IELs, we analyzed the
241 αβTCR clonotypes expressed by T cells in the small and large intestine, mammary gland and
242 spleen. First, we used single-cell TCRseq to compare αβTCR pairs displayed by IELs (small and
243 large intestine) and mammary gland T cells in the same mice (four nulliparous and four lactating,
244 21,750 total cells). Overall, the data showed unremarkable V and J region usage, CDR3 length and
245 N region diversity frequencies. Canonical TRAV11/TRAJ18 TCRs of iNKT cells were relatively
246 abundant among lactating mammary T cells, mostly in CD4-CD8- DNs (2.2 and 8.1% of total
247 cells, Fig. S9A). Rarefaction analysis revealed a notable degree of clonal amplification in different
248 T cell-types from the lactating mammary gland compared to the nulliparous mammary gland;
249 whereas amplification is seen in both the lactating and nulliparous small intestine (Fig. 5A, S9B),
250 but with much mouse-to-mouse variation. We identified 13 TCR clonotypes shared between small
251 intestine and mammary T cells in lactating mice, in contrast to 3 shared TCR clonotypes in
252 nulliparous mice (Fig. 5B,C and Table S1). These shared clonotypes were defined by full
253 nucleotide sequence identity, and were completely absent when comparing different mice,
254 indicating that they stemmed from the same T cell clones present in both mammary gland and
255 small intestine (and large intestine, for some). The clonotypes shared with the intestines accounted
256 for 4.3% and 0.6% of mammary T cells in the two lactating mice, certainly an underestimate given

incomplete sampling. As indicated in Fig. 5C and Table S1, clonotypes present in both small intestine and mammary gland belonged to several cell types, indicating that the exchange between tissues involves different T lineages. Some clonotypes shared between intestine and mammary gland were also observed in nulliparous females (2.2% and 0.9% of mammary T cells in the two mice profiled). Thus, exchanges of T cells between intestine and mammary gland pre-exist the onset of lactation.

These clonotypic analyses also revealed the sharing of a particular intriguing group of cells. For a broader comparison of small intestine cells, we leveraged TCR sequence data of intestinal IELs generated in the ImmGenT program[45], and used the TCRdist3 algorithm[46] to compute a matrix of distances between αβTCR clonotypes. This revealed two prominent TCR families within the small intestinal IEL compartment (Fig. 5D), whose over-representation was striking because of the recruitment of highly related TCRs with little clonal amplification, as denoted by subtly different nucleotide sequences. These TCR families were found in many independent samples, and one indeed corresponded to the previously reported "Revere" family[47] (we hereafter name the second family "Newbury" for consistency). Revere TCRs are mostly conserved in the CDR3b region, with exclusive usage of TRAJ22 and TRBJ1-4 (Fig. 5E, S10A), while the Newbury family is mostly conserved in the CDR3a region. Notably, these two families are almost exclusively represented in the intestinal CD8αα+ IELs, amounting to a few percent of T cells (Fig. S10B, C), and these highly identical TCRs of the CD8αα+ IELs are likely selected repeatedly by self-reactivity, in line with well-known selection of CD8αα differentiation by self-reactive transgenic TCRs[34, 35, 36]. Interestingly, Revere and Newbury TCRs were also observed in CD8αα+ IELs of the mammary gland (3 of each), with all the key sequence characteristics (Fig. 5F, S10D). Thus, peculiar TCR families of intestinal CD8αα+ IELs are found in IELs of the lactating mammary gland. Importantly, outside of the intestine and mammary gland, CD8αα+ IELs did not display Revere or Newbury family TCRs, as analyzed by the immgenT program (Fig. 5G, chisq.test $p=6.10^{-4}$)). Together, CD8αα+ IELs in the lactating mammary gland displayed TCRs otherwise exclusive to intestinal IELs, as part of a broader exchange of T cell clones between the intestine and mammary gland.

***IEL-like cells are present in human mammary gland and human milk.***

287 We assessed whether mammary IELs were conserved across species by profiling T cells in human
288 breast tissue and human milk. First, we used previously published scRNAseq datasets[48] and found
289 that human breast tissue from non-lactating women contains naïve (*SELL*) T cells as well as CD4+
290 and CD8αβ+ T cells that express tissue resident and cytotoxic markers expressed by mouse
291 mammary IELs including *ITGAE*, *CD94*, *CD160*, *NKG2D,* and *GZMB* (Fig. 6A,B, S11A). We also
292 observed a small population of cells that expressed genes associated with CD8αα+ IELs including
293 *FCER1G* and *TYROBP.* The presence of CD4+ and CD8+ T cells in milk has been reported
294 before[25], but with no further characterization. To ask whether human milk contains CD8αα+ IEL-
295 like cells in addition to the other subsets, we analyzed fresh milk samples from lactating women.
296 Multiparameter flow cytometry revealed both CD4+ and CD8+ T cells in all samples. In addition,
297 CD8αα+ IEL-like cells in human milk, including cells that expressed CD103, CD94, and NKG2D
298 (Fig. 6C-E). Overall, we identified human counterparts of mouse mammary IELs in human breast
299 and milk.

300 ***Microbiota influence numbers and activation states of mammary IELs.***

301 The classical function of IELs is to maintain barrier immunity, which raised the question of
302 microbe-dependence of IELs in the lactating mammary gland, considering the transition involves
303 exposure to environmental microbes. Lactating mammary glands in microbe-deficient germ-free
304 (GF) mice had morphologically different ducts compared to microbe-sufficient (specific pathogen
305 free, SPF) control mice in hematoxylin-eosin stained sections (Fig. 7A). Although the number of
306 mammary alveoli in SPF and GF mice were comparable, the average area ($um^2$) of GF alveoli was
307 larger, indicating that microbes may affect the developmental progression of the mammary gland
308 during lactation (Fig. 7B, C). Microbes influenced total mammary immunocytes, as indicated by
309 fewer total CD45+ cells in GF mice (Fig. 7D), but there were no differences in the proportion of
310 basal or luminal epithelial cells between GF and SPF mice (Fig. S11B). There was also no
311 significant difference in the average pup weight normalized to litter size (Fig. S11C), but whether
312 microbes influence milk composition or production needs to be further investigated.

313 GF mice showed decreased numbers of CD4+ Teff, CD8αα+ Teff, and CD8αβ+ IELs
314 compared to SPF mice (Fig. 7E). However, the proportions of T cell types were not different
315 between the groups suggesting that the decrease in IEL numbers was due to the total drop in CD45+
316 cells (Fig. S11D). The decrease in mammary IELs could also stem from decreased intestinal IELs,

317 as GF mice display a significant decrease in CD4+ IELs and CD8αβ+ IELs, and a modest decrease
318 in intestinal CD8αα+ IELs[49]. The defect in mammary IELs may arise from migrating intestinal
319 IELs that lack the same functionality, reflecting the role of intestinal microbes in priming
320 mammary IELs. To test the role of intestinal microbes, we conventionalized GF mice by
321 transferring fecal microbes from control SPF mice into GF mice at 6 weeks of age.
322 Conventionalized GF mice displayed increased CD45+ cells during lactation, including restoration
323 of the mammary IEL populations (Fig. 7D,E). To further analyze micro-dependent phenotypic
324 changes, we performed multiplexed scRNAseq on T cells from lactating mammary glands from
325 GF or SPF mice (Fig. 7F, 13,021 cells, 8 mice, 2 independent runs). All mammary IEL populations
326 were equally represented in the two groups consistent with quantitation by flow cytometry (Fig.
327 7F). Differential gene expression between SPF and GF IELs showed few transcriptional
328 differences, including significant changes in *Itgb1, Igf1r, Ikzf2, Tnfaip3, Thy1*, and *Klra9* (Fig.
329 7G). While several of these genes are immunomodulatory, whether these changes affect the
330 function of mammary IELs in GF mice needs to be examined. Thus, our data points to the
331 importance of commensal microbes in modulating numbers of mammary gland IELs during
332 lactation.

333

334 **DISCUSSION**

335 We report a dynamic atlas of T cells whose changes accompany the adaptation of the mammary
336 gland to a mucosal state in lactation, with an increase in activated CD4+, CD8αβ+ and CD8αα+
337 T cells that are intraepithelial in location. Mammary CD8αα+ IELs shared TCR clonotypes with
338 intestinal CD8αα+ TCRαβ+ IELs, suggesting T cell migration from the intestine to the mammary
339 gland. Mammary IELs may be conserved across species since human breast tissue and milk
340 contained T cells with a similar signature. Finally, we found that T cell numbers and activation in
341 lactation were partly influenced by microbes, suggesting that the observed T cell changes could be
342 geared towards promoting barrier immunity during lactation.

343 Intestinal IEL subsets maintain and protect the intestinal barrier[31], functions that mammary IELs
344 could be involved in to promote lactogenesis. The TCR specificity of CD8αα+ IELs is directed
345 towards self-antigens[34, 35, 36], and in line with that, we found two families of TCRs that are

346 repeatedly generated and selected across mice, and were found in the small intestine and lactating
347 mammary gland. CD8αα homodimers have been shown to function as TCR corepressors by
348 binding to TL (thymus leukemia) antigen on epithelial cells, to negatively regulate T cell activation
349 by decreasing antigen sensitivity, in contrast to CD8αβ heterodimers that enhance TCR function[50].
350 Our results suggest that mammary CD8αα+ IELs are poised to respond to the rapid epithelial cell
351 proliferation, or to the plethora of self-antigens that are present in the lactating mammary gland,
352 but whether their function is tolerogenic or cytotoxic needs to be determined. During pregnancy
353 and lactation, the expression of gut-homing markers Ccl25, Ccl28, and MAdCAM1, increase in
354 the mammary tissue which could lead to T cell migration to the mammary gland[22, 51, 52]. However,
355 whether the expression of these homing markers change in the intestine during pregnancy and
356 lactation which mediate T cell egress, and whether hormones influence mammary homing markers
357 needs to be further explored.

358 Apart from their physiological role in lactogenesis, CD8αα+ IELs may influence post-lactation
359 oncogenesis. Similar populations of NK-like unconventional T cells such as αβILTCKs and NK-
360 like γδ T cells, have been shown to be important in suppressing mammary oncogenesis[26, 32].
361 Mammary T cells are present in human milk where function, if any, is unclear. One possibility is
362 that their presence is passive, and linked to epithelial cell sloughing in lactogenesis, which
363 increases epithelium-associated T cells in milk. Maternal T cells have been previously suggested
364 to colonize neonatal intestines[53], raising the other possibility that milk IELs could migrate into and
365 colonize the neonatal intestine to promote barrier protection.

366 Pregnancy induces an immunosuppressive state to maintain maternal-fetal tolerance and support
367 successful pregnancy outcomes[54]. However, in the mammary gland, we observe an increase in
368 effector T cell populations in late pregnancy and early lactation presumably to prepare for
369 increased microbial exposure or increased epithelial cell proliferation in lactation. Consistent with
370 the idea of increased microbial exposure, activated T cells decrease in the GF mammary gland,
371 and the drop in mammary Tregs in lactating SPF mice is not observed in GF mice (Fig. S11E).
372 Interestingly, liMacs were also reduced in lactating GF mammary glands[17], suggesting that
373 microbes or microbe-derived signals can influence multiple immunocyte-types involved in
374 mammary remodeling.

375 In summary, we have characterized novel T cell changes during lactogenesis and provide evidence
376 for T cell migration potentially along the entero-mammary axis. Our results set the stage for
377 deepening our understanding of T cell function in lactogenesis, which could provide new strategies
378 to improve maternal defense and tolerance during and after lactation.

379

380 **METHODS**

381 **Mice**

382 C57BL/6 (B6) mice were purchased from Jackson Labs and maintained in specific pathogen free
383 (SPF) conditions at Harvard Medical School and Salk Institute for Biological Sciences.
384 Nulliparous mice were littermate controls of mice profiled at pregnancy, lactation, or involution.
385 For timed pregnancies, female B6 mice were set up at 6-8 wks of age with male B6 mice, female
386 mice with plugs were separated and housed individually for the duration of pregnancy, and
387 mammary glands were profiled at day 12 (G12), day 17 (G17) of pregnancy, lactation day 3-5
388 (L3), and involution day 1 (I), one day post-weaning of pups at day 21. All experiments were
389 performed following guidelines listed in animal protocols (IS00001257, Harvard Medical School)
390 and (23-00007**,** Salk Institute for Biological Studies) approved by the Institutional Animal Care
391 and Use Committee.
392 Germ free (GF) B6 mice were purchased at timepoints listed above from the University of
393 California San Diego. GF mice were conventionalized by oral gavage of fecal microbiota from
394 SPF B6 mice, one week prior to mating and maintained in SPF conditions.
395 Kaede reporter mice were obtained from O. Kanagawa (RIKEN, Wako, Japan) and maintained
396 on the B6 background[55, 56].

397

398 **Preparation of lymphocytes and flow cytometry.**

399 Mammary gland: Inguinal lymph nodes were removed and mammary glands 3, 4 and 5 were
400 collected, minced and dissociated in collagenase solution (3mg/mL collagenase type II (Sigma
401 C6885) and 2% FBS in DMEM) in a 37˚C shaking water bath for 20 min with manual shaking
402 every 5 min, followed by red blood cell lysis. Single cell suspensions were filtered and washed
403 with 2% DMEM solution.

404 Thymus and LN: Lymphocytes from thymus and inguinal lymph nodes were obtained by
405 mechanical disruption, filtered and washed with 10% RPMI solution.
406 Intestines: Small and large intestinal tissues were measured, cleaned, and treated with RPMI
407 containing 1mM DTT, 20mM EDTA and 2% FBS at 37˚C for 15 min to isolate the epithelial and
408 IEL fractions. For the lamina propria (LP) fraction, the remaining tissue was dissociated in
409 collagenase solution (1 mg/mL collagenase VIII (Sigma C2139), 50μg/ml DNase (Sigma C6885)
410 in 1%FBS in RPMI) with constant stirring at 37˚C for 30min. Single cell suspensions for the IEL
411 and LP fractions were filtered and washed with 10% RPMI solution.
412 Spleen: Tissue was mechanically disrupted, followed by red blood cell lysis. Single cell
413 suspensions were filtered and washed with 10% RPMI solution.
414 Staining: Single cell suspensions of cells resulting from tissue dissociations were stained with
415 different panels of antibodies with surface markers for CD45, CD4, CD8α, CD8β, TCRβ, TCRδ,
416 NK1.1, Ly49, CD103, Thy1, PD-1, CD122, CD5, CD69, CD44, CD62L, CD38, CD244, and
417 CD160 Zombie UV Fixable Viability and intracellular markers for T-bet, Ki67 and Foxp3. For
418 intracellular staining, cells were stained for surface markers and fixed in eBioscience Fix/Perm
419 buffer overnight, followed by permeabilization in eBioscience permeabilization buffer at room
420 temperature for 45 min in the presence of antibodies. Cells were acquired with a BD LSRII or BD
421 FACSymphony A3 and analysis was performed with FlowJo 10 software.

422

423 **Photoconversion Procedure**

424 Kaede transgenic mice were anesthetized, abdomen was surgically opened and a portion
425 (approximately one third in non-pregnant mice, smaller portion in pregnant mice) of the small
426 intestine was exposed. The mouse, except for the small intestine, was covered in aluminum foil
427 and the small intestine was exposed to a handheld 405 nm blue purple laser for 30 second light
428 pulses (which converts Kaede green cells to Kaede red). After photoconversion the mouse was
429 surgically closed and sacrificed 24 hours later for flow cytometry analysis of Kaede green vs Kaede
430 red cells.

431

432 **Single cell RNA and TCR sequencing**

433 Mammary immunocytes: Live CD45+ cells were sorted from the mammary gland of nulliparous
434 (n=6), gestation day 17 (n=4), lactation day 3-5 (n=6), and involution (n=4) mice using a BD
435 FACSAria after hashtagging with Biolegend TotalSeq-A reagents, and samples were pooled for
436 encapsulation (10X Chromium). Libraries were prepared using Chromium Single cell 3' reagents
437 kit v2 and sequenced on NovaSeq 6000.
438 Multi-organ combined scRNAseq and TCRseq: Live T cells (DAPI-CD3+CD44+TCRβ+) were
439 sorted from the mammary gland, small intestines, large intestines, spleen and thymus from
440 nulliparous (n=4) and lactation day 4 (n=4) mice. The cells were hashtagged with Biolegend
441 TotalSeq-C reagents and pooled for encapsulation (10X Chromium). Libraries were prepared
442 using Chromium Single cell 5' reagents kit v3 and sequenced on NovaSeq 6000. TCR and hashtag
443 libraries were processed as described[29].
444 Germ-free vs SPF: Live T cells (DAPI-CD3+CD44+TCRβ+) were sorted from GF (n=4) and SPF
445 (n=4) mammary glands on lactation day 4. Samples were pooled for encapsulation (10X
446 Chromium), libraries were prepared using Chromium Single cell 3' reagents kit v3 and sequenced
447 on NovaSeq 6000.
448 Epithelial-IEL interactions: Live EpCAM+ CD45-, CD45+ EpCAM- cells, and TCRβ+ cells were
449 sorted, pooled for encapsulation (10X Chromium), libraries prepared using Chromium Single cell
450 3' reagents kit v3 and sequenced on NovaSeq 6000.
451 Single-cell RNAseq data was analyzed using the Seurat pipeline, which allowed for data
452 normalization, clustering, and identification of differentially expressed genes across groups.
453
454 **Cell Interaction Predictions:**

455 CellChat v2 was used to infer and visualize intercellular communication networks in the mammary
456 gland[40, 57]. CellChat v2 is an R package that is able to predict and analyze intercellular
457 communication pathways from single-cell data. The analysis was done as described in the CellChat
458 v2 published protocol. Briefly, EpCAM+ and TCRβ+ cells were isolated from the scRNA-seq data
459 and used to predict intercellular communication pathways. To perform comparison analysis, we
460 isolated differentially expressed ligands and receptors between nulliparous and lactating mice ($p$
461 $< 0.05$), which were used to predict communication pathways that could be different between these
462 groups. For visualization purposes, the networks between EpCAM+ and TCRβ+ cells were

463 isolated and visualized using chord diagrams. Summary of signaling pathways were generated
464 using CellChat v2 and visualized using chord diagrams.
465
466 **Histology, Imaging and Microscopy**
467 Mammary gland 4 was harvested from nulliparous, gestation (G17), lactation (L3-5), and
468 involution (I) stages and fixed in 4% Paraformaldehyde (PFA) solution in PBS overnight at 4°C
469 shaking. They were washed with PBS and stored in 70% ethanol prior to being embedded in
470 paraffin. Immunofluorescence staining was performed as previously described[58]. All primary
471 antibodies were diluted in Renaissance Background reducing diluent (Biocare, PD905L). All opals
472 were diluted 1:500 in 1X Plus Manual Amplification Diluent (Akoya Biosciences, FP1498).

473 Microscopy methods are reported following the guidance of (Montero-llopis et al, 2021)[59] for best
474 reproducible practices. Images in Figures 2E and S4D were acquired using an Olympus VS200
475 Slide Scanner widefield microscope equipped with a NOCEM X-cite light source (405-780nm)
476 and the fluorescent camera Hamamatsu Orca fusion BTsCMOS (2304x2304 pixels 6.5 um).
477 Images were acquired using a UPlan X Apo 20x/0.8 air objective. Signal from DAPI, FITC,
478 TRITC, CY5 and CY7 was collected by illuminating the sample using the FF409/493/573/652-
479 Di02 or FF757-Di01 multiband dichroics and the following excitation (FF01-378/52, FF01-
480 474/27, FF01-554/23, FF01-635/18, FF01-735/28) and emission (FF01-432/36, FF01-515/30,
481 FF01-595/31, FF01-698/70, FF02-809/81) filters respectively. Images were acquired using the
482 OlyVIA software from Olympus and processed by Qpath and FIJI to crop representative areas and
483 threshold background signal.

484 For H&E staining, sections were deparaffinized, stained with hematoxylin and eosin, dehydrated
485 and mounted with coverslips and imaged on an Olympus upright INSERT SCOPE brightfield
486 microscope at 10x and 20x magnification.
487 <u>Milk Alevoli Quantification:</u> Milk duct area was measured using Fiji to measure each duct in 4
488 different 20x magnification images per mouse and the average of all ducts was calculated.
489
490 **Human Milk**
491 5 mL of human milk were received from UC San Diego HMB Biorepository and diluted 1:1 with
492 PBS. Milk samples were centrifuged to remove lipid and whey layers. Remaining cells were

493 stained using viability dye, CD4, CD94, CD8β, CD3, TCRδ, CD44, CD45, CD8α, CD103, and
494 NKG2D. Cells were analyzed using BD LSRFortessa or BD FACSymphony A3 and analysis
495 was performed with FlowJo 10 software. The protocol for analysis of human milk samples was
496 approved by the UCSD Institutional Review Board Administration (IRB number: 808920) and
497 patients provided written informed consent prior to enrollment.

498

499 **Quantification and Statistical Analysis**

500 Data are presented as mean ± SEM. Unless stated otherwise, significance was assessed by
501 Student's t-test or one-way Anova in GraphPad Prism 8.0.

502

503 **Data availability**

504 Single cell sequencing data are available in NCBI with accession numbers GSE290256 and
505 GSE288901. Mammary gland T cell data are available in a user-friendly format at

506 https://cbdm.connect.hms.harvard.edu/ImmgenT/PublicRosetta/

507

508 **ACKNOWLEDGEMENTS**

509 We would like to thank Gabriel Ascui-Gac and Dr. Mitchell Kronenburg for reagents and advise
510 on MAIT cell analysis, and Dr. Queralt Vallmajo Martin and Dr. Danish Umar for helpful
511 discussions. This work was supported by NIH grants RO1-AI150686 to CB, R24-072073 to the
512 ImmGen Consortium, NIH-NCI CCSG: P30 CA01495, and Shared Instrumentation Grants S10-
513 OD023689 to the Salk Institute core facilities (FCCF, NGS).

514

515 **ImmgenT consortium members:** David Zemmour, Christophe Benoist, Dania Mallah, Ian
516 Magill, Liang Yang, Ananda Goldrath, Joonsoo Kang, Mitch Kronenberg, Nika Abdollahi, Myriam
517 Croze, Serge Candéias, Sofia Kossida, Véronique Giuducelli, Sam Behar, Remy Bosselut, Laurent
518 Brossay, Ken Cadwell, Alexander Chervonsky, Laurent Gapin, Jun Huh, Iliyan Iliev, Bana Jabri,
519 Steve Jameson, Marc Jenkins, Susan Kaech, Dan Kaplan, Vijay Kuchroo, Stefan Muljo, Michel
520 Nussenzweig, Marion Pepper, David Sinclair, Michael Starnbach, Paul Thomas, Ulrich von

Andrian, Derek Bangs, Olga Barreiro del Rio, Gavyn Bee, Katharine Block, Sam Borys, Evelyn Chang, Josh Choi, Enxhi Ferraj, Giovanni Galletti, Lizzie Garcia-Rivera, Anna-Maria Globig, Xutong Gong, Takato Kusakabe, Rocky Lai, Andrea Lebron-Figueroa, Woan-Yu Lin, Mariya London, Erin Lucas, Ankit Malik, Julia Merkenschlager, Nathan Morris, Kevin Osum, Jinseok Park, Val Piekarsa, Sara Quon, Shanelle Reilly, Stefan Schattgen, Tomoyo Shinkawa, Nalat Siwapornchai, Claire Thefane, Melanie Vacchio, Jordan Voisine, Eric Weiss, Alia Welsh, Shanshan Zhang.

## REFERENCES

1. Joshi, P.A. *et al.* Progesterone induces adult mammary stem cell expansion. *Nature* **465**, 803-807 (2010).

2. Asselin-Labat, M.L. *et al.* Control of mammary stem cell function by steroid hormone signalling. *Nature* **465**, 798-802 (2010).

3. Dulbecco, R., Henahan, M. & Armstrong, B. Cell types and morphogenesis in the mammary gland. *Proc Natl Acad Sci U S A* **79**, 7346-7350 (1982).

4. Hassiotou, F. & Geddes, D. Anatomy of the human mammary gland: Current status of knowledge. *Clin Anat* **26**, 29-48 (2013).

5. Watson, C.J. & Khaled, W.T. Mammary development in the embryo and adult: a journey of morphogenesis and commitment. *Development* **135**, 995-1003 (2008).

6. Bach, K. *et al.* Differentiation dynamics of mammary epithelial cells revealed by single-cell RNA sequencing. *Nat Commun* **8**, 2128 (2017).

7. Nyquist, S.K. *et al.* Cellular and transcriptional diversity over the course of human lactation. *Proc Natl Acad Sci U S A* **119**, e2121720119 (2022).

8. Li, M. *et al.* Mammary-derived signals activate programmed cell death during the first stage of mammary gland involution. *Proc Natl Acad Sci U S A* **94**, 3425-3430 (1997).

9. Watson, C.J. Involution: apoptosis and tissue remodelling that convert the mammary gland from milk factory to a quiescent organ. *Breast Cancer Res* **8**, 203 (2006).

10. Lilla, J.N. & Werb, Z. Mast cells contribute to the stromal microenvironment in mammary gland branching morphogenesis. *Dev Biol* **337**, 124-133 (2010).

11. Gouon-Evans, V., Rothenberg, M.E. & Pollard, J.W. Postnatal mammary gland development requires macrophages and eosinophils. *Development* **127**, 2269-2282 (2000).

12. Dawson, C.A. *et al.* Tissue-resident ductal macrophages survey the mammary epithelium and facilitate tissue remodelling. *Nat Cell Biol* **22**, 546-558 (2020).

13. O'Brien, J., Martinson, H., Durand-Rougely, C. & Schedin, P. Macrophages are crucial for epithelial cell death and adipocyte repopulation during mammary gland involution. *Development* **139**, 269-275 (2012).

14. Pollard, J.W. & Hennighausen, L. Colony stimulating factor 1 is required for mammary gland development during pregnancy. *Proc Natl Acad Sci U S A* **91**, 9312-9316 (1994).

15. Ingman, W.V., Wyckoff, J., Gouon-Evans, V., Condeelis, J. & Pollard, J.W. Macrophages promote collagen fibrillogenesis around terminal end buds of the developing mammary gland. *Dev Dyn* **235**, 3222-3229 (2006).

16. Reed, J.R. & Schwertfeger, K.L. Immune cell location and function during post-natal mammary gland development. *J Mammary Gland Biol Neoplasia* **15**, 329-339 (2010).

17. Cansever, D. *et al.* Lactation-associated macrophages exist in murine mammary tissue and human milk. *Nat Immunol* **24**, 1098-1109 (2023).

18. Ramanan, D. *et al.* An Immunologic Mode of Multigenerational Transmission Governs a Gut Treg Setpoint. *Cell* **181**, 1276-1290 e1213 (2020).

19. Roux, M.E., McWilliams, M., Phillips-Quagliata, J.M., Weisz-Carrington, P. & Lamm, M.E. Origin of IgA-secreting plasma cells in the mammary gland. *J Exp Med* **146**, 1311-1322 (1977).

20. Roux, M.E., McWilliams, M., Phillips-Quagliata, J.M. & Lamm, M.E. Differentiation pathway of Peyer's patch precursors of IgA plasma cells in the secretory immune system. *Cell Immunol* **61**, 141-153 (1981).

21. Lazarus, N.H. *et al.* A common mucosal chemokine (mucosae-associated epithelial chemokine/CCL28) selectively attracts IgA plasmablasts. *J Immunol* **170**, 3799-3805 (2003).

22. Wilson, E. & Butcher, E.C. CCL28 controls immunoglobulin (Ig)A plasma cell accumulation in the lactating mammary gland and IgA antibody transfer to the neonate. *J Exp Med* **200**, 805-809 (2004).

23. Plaks, V. *et al.* Adaptive Immune Regulation of Mammary Postnatal Organogenesis. *Dev Cell* **34**, 493-504 (2015).

24. Betts, C.B. *et al.* Mucosal Immunity in the Female Murine Mammary Gland. *J Immunol* **201**, 734-746 (2018).

25. Wirt, D.P., Adkins, L.T., Palkowetz, K.H., Schmalstieg, F.C. & Goldman, A.S. Activated and memory T lymphocytes in human milk. *Cytometry* **13**, 282-290 (1992).

26. Hanasoge Somasundara, A.V. *et al.* Parity-induced changes to mammary epithelial cells control NKT cell expansion and mammary oncogenesis. *Cell Rep* **37**, 110099 (2021).

27. Butler, A., Hoffman, P., Smibert, P., Papalexi, E. & Satija, R. Integrating single-cell transcriptomic data across different conditions, technologies, and species. *Nat Biotechnol* **36**, 411-420 (2018).

28. Crowl, J.T. *et al.* Tissue-resident memory CD8(+) T cells possess unique transcriptional, epigenetic and functional adaptations to different tissue environments. *Nat Immunol* **23**, 1121-1131 (2022).

29. Kiner, E. *et al.* Gut CD4(+) T cell phenotypes are a continuum molded by microbes, not by T(H) archetypes. *Nat Immunol* **22**, 216-228 (2021).

30. Denning, T.L. *et al.* Mouse TCRalphabeta+CD8alphaalpha intraepithelial lymphocytes express genes that down-regulate their antigen reactivity and suppress immune responses. *J Immunol* **178**, 4230-4239 (2007).

31. Cheroutre, H., Lambolez, F. & Mucida, D. The light and dark sides of intestinal intraepithelial lymphocytes. *Nat Rev Immunol* **11**, 445-456 (2011).

633 32. Chou, C. *et al.* Programme of self-reactive innate-like T cell-mediated cancer immunity.
634 *Nature* **605**, 139-145 (2022).

635
636 33. Ruscher, R. & Hogquist, K.A. Development, ontogeny, and maintenance of
637 TCRalphabeta(+) CD8alphaalpha IEL. *Curr Opin Immunol* **58**, 83-88 (2019).

638
639 34. Leishman, A.J. *et al.* Precursors of functional MHC class I- or class II-restricted
640 CD8alphaalpha(+) T cells are positively selected in the thymus by agonist self-peptides.
641 *Immunity* **16**, 355-364 (2002).

642
643 35. Gangadharan, D. *et al.* Identification of pre- and postselection TCRalphabeta+
644 intraepithelial lymphocyte precursors in the thymus. *Immunity* **25**, 631-641 (2006).

645
646 36. Hogquist, K.A., Baldwin, T.A. & Jameson, S.C. Central tolerance: learning self-control in the
647 thymus. *Nat Rev Immunol* **5**, 772-782 (2005).

648
649 37. Brenes, A.J. *et al.* Tissue environment, not ontogeny, defines murine intestinal
650 intraepithelial T lymphocytes. *Elife* **10** (2021).

651
652 38. Kornberg, A. *et al.* Gluten induces rapid reprogramming of natural memory alphabeta and
653 gammadelta intraepithelial T cells to induce cytotoxicity in celiac disease. *Sci Immunol* **8**,
654 eadf4312 (2023).

655
656 39. Jaeger, N. *et al.* Single-cell analyses of Crohn's disease tissues reveal intestinal
657 intraepithelial T cells heterogeneity and altered subset distributions. *Nat Commun* **12**,
658 1921 (2021).

659
660 40. Jin, S. *et al.* Inference and analysis of cell-cell communication using CellChat. *Nat Commun*
661 **12**, 1088 (2021).

662
663 41. Hou, Z. *et al.* Glycosylation-dependent cell adhesion molecule 1 (GlyCAM 1) is induced by
664 prolactin and suppressed by progesterone in mammary epithelium. *Endocrinology* **141**,
665 4278-4283 (2000).

666
667 42. Alain, K. *et al.* Osteopontin: an early innate immune marker of Escherichia coli mastitis
668 harbors genetic polymorphisms with possible links with resistance to mastitis. *BMC*
669 *Genomics* **10**, 444 (2009).

670

671 43. Ruscher, R., Kummer, R.L., Lee, Y.J., Jameson, S.C. & Hogquist, K.A. CD8alphaalpha
672 intraepithelial lymphocytes arise from two main thymic precursors. *Nat Immunol* **18**, 771-
673 779 (2017).

674

675 44. Galvan-Pena, S., Zhu, Y., Hanna, B.S., Mathis, D. & Benoist, C. A dynamic atlas of
676 immunocyte migration from the gut. *Sci Immunol* **9**, eadi0672 (2024).

677

678 45. Zemmour, D., Goldrath, A., Kronenberg, M., Kang, J. & Benoist, C. The ImmGen consortium
679 OpenSource T cell project. *Nat Immunol* **23**, 643-644 (2022).

680

681 46. Mayer-Blackwell, K. *et al.* TCR meta-clonotypes for biomarker discovery with tcrdist3
682 enabled identification of public, HLA-restricted clusters of SARS-CoV-2 TCRs. *Elife* **10**
683 (2021).

684

685 47. Stefan A Schattgen, J.C.C., Lee-Ann Van de Velde, Hiutung Chu, Sarkis K Mazmanian, Phil
686 Bradley, Paul G Thomas. Intestinal intraepithelial lymphocyte repertoires are imprinted
687 clonal structures selected for MHC reactivity. *Cell Press Sneak Peek* (2019).

688

689 48. Kumar, T. *et al.* A spatially resolved single-cell genomic atlas of the adult human breast.
690 *Nature* **620**, 181-191 (2023).

691

692 49. Sujino, T. *et al.* Tissue adaptation of regulatory and intraepithelial CD4(+) T cells controls
693 gut inflammation. *Science* **352**, 1581-1586 (2016).

694

695 50. Cheroutre, H. & Lambolez, F. Doubting the TCR coreceptor function of CD8alphaalpha.
696 *Immunity* **28**, 149-159 (2008).

697

698 51. Brandtzaeg, P. The mucosal immune system and its integration with the mammary glands.
699 *J Pediatr* **156**, S8-15 (2010).

700

701 52. Low, E.N., Zagieboylo, L., Martino, B. & Wilson, E. IgA ASC accumulation to the lactating
702 mammary gland is dependent on VCAM-1 and alpha4 integrins. *Mol Immunol* **47**, 1608-
703 1612 (2010).

704

705 53. Cabinian, A. *et al.* Transfer of Maternal Immune Cells by Breastfeeding: Maternal Cytotoxic
706 T Lymphocytes Present in Breast Milk Localize in the Peyer's Patches of the Nursed Infant.
707 *PLoS One* **11**, e0156762 (2016).

708

54. Erlebacher, A. Immunology of the maternal-fetal interface. *Annu Rev Immunol* **31**, 387-411 (2013).

55. Tomura, M. *et al.* Monitoring cellular movement in vivo with photoconvertible fluorescence protein "Kaede" transgenic mice. *Proc Natl Acad Sci U S A* **105**, 10871-10876 (2008).

56. Morton, A.M. *et al.* Endoscopic photoconversion reveals unexpectedly broad leukocyte trafficking to and from the gut. *Proc Natl Acad Sci U S A* **111**, 6696-6701 (2014).

57. Jin, S., Plikus, M.V. & Nie, Q. CellChat for systematic analysis of cell-cell communication from single-cell transcriptomics. *Nat Protoc* **20**, 180-219 (2025).

58. Sorrelle, N. *et al.* Improved Multiplex Immunohistochemistry for Immune Microenvironment Evaluation of Mouse Formalin-Fixed, Paraffin-Embedded Tissues. *J Immunol* **202**, 292-299 (2019).

59. Montero Llopis, P. *et al.* Best practices and tools for reporting reproducible fluorescence microscopy methods. *Nat Methods* **18**, 1463-1476 (2021).

Figure 1

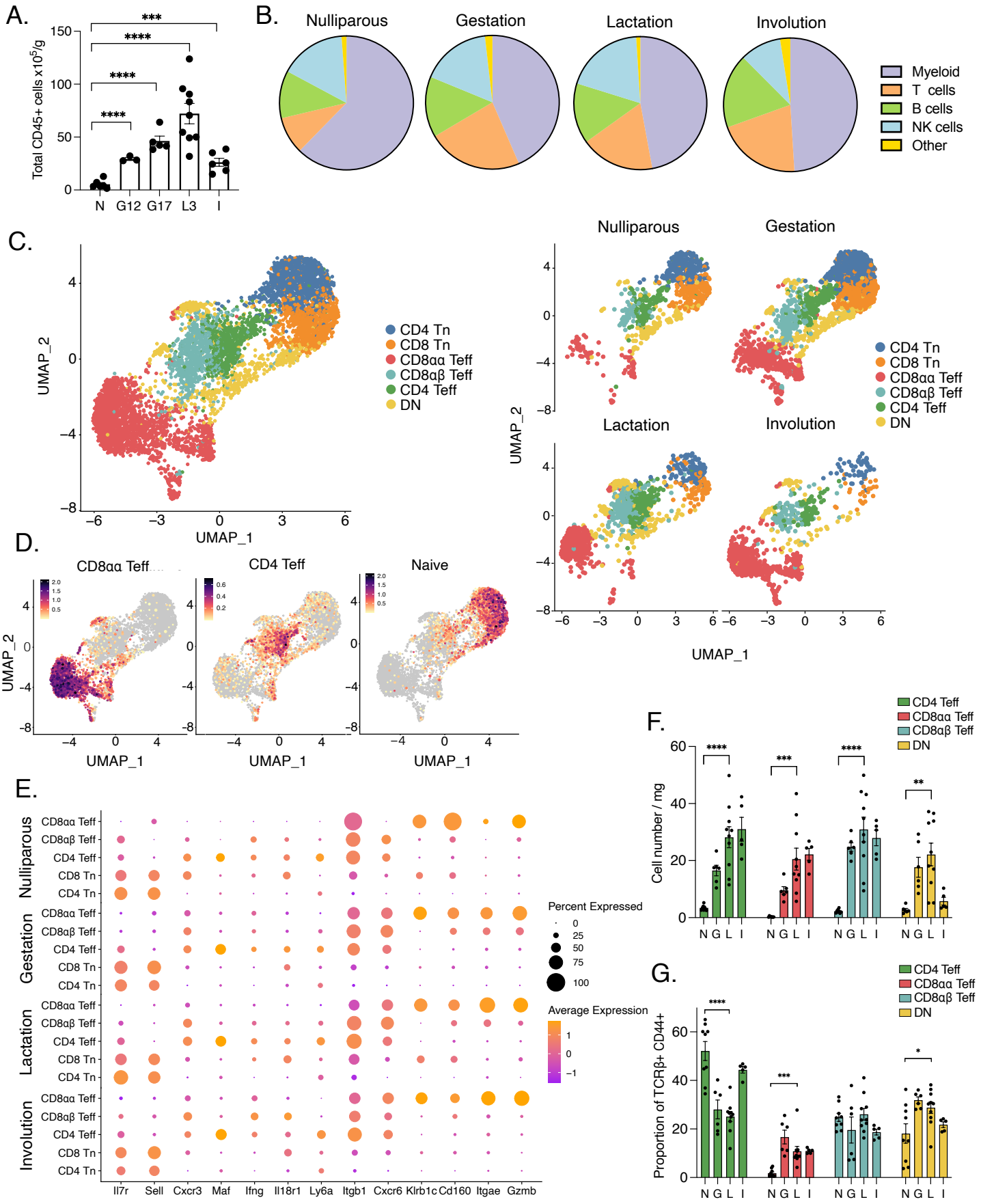
A.
Total CD45+ cells x10^5/g
N
G12
G17
L3
I
B.
Nulliparous
Gestation
Lactation
Involution
Myeloid
T cells
B cells
NK cells
Other
C.
UMAP_1
UMAP_2
CD4 Tn
CD8 Tn
CD8αα Teff
CD8αβ Teff
CD4 Teff
DN
D.
CD8αα Teff
CD4 Teff
Naive
E.
Nulliparous
Gestation
Lactation
Involution
Il7r
Sell
Cxcr3
Maf
Ifng
Il18r1
Ly6a
Itgb1
Cxcr6
Klrb1c
Cd160
Itgae
Gzmb
Percent Expressed
Average Expression
F.
Cell number / mg
G.
Proportion of TCRβ+ CD44+

**Figure 1. Late gestation and lactation lead to increased Teff populations in the mammary gland.**

A) Quantification of total number of CD45+ cells normalized to mammary gland weight across stages of gestation and lactation by flow cytometry. N=nulliparous (n=6), G12=gestation day 12 (n=3), G17=gestation day 17 (n=5), L3=lactation days 3-5 (n=9), and I=involution, 1 day post weaning (n=6).

B) Representative proportions of major immune cell types in the mammary gland across stages, nulliparous (n=5), gestation (n=3), lactation (n=5), and involution (n=5), quantified by flow cytometry.

C) UMAP projection of mammary T cells. Split by stages: nulliparous, gestation (G17), lactation (L3), and involution (right). Representative UMAP is from one of three independent experiments, n=3.

D) Feature plots of CD8αα Teff, CD4 Teff and Naïve T cells from (C).

E) Dot plot of selected highly expressed genes in T cell clusters across stages identified in (C). Dot size represents the percentage of cells expressing the selected gene and color indicates expression level.

F-G) Quantification by flow cytometry of cell numbers (F) and proportions (G) of T cell populations identified in (C) normalized to mammary gland weight. Teff populations were determined as CD4 Teff: CD4+CD44+CD62L-. CD8αα Teff: CD8α+CD8β-CD44+CD62L-. CD8αβ Teff: CD8α+CD8β+CD44+CD62L-. DN: TCRβ+CD4-CD8α-. N=nulliparous (n=8, n=6 for DN), G=gestation (n=6), L=lactation (n=10) and I=involution (n=5).

**$p<0.01$, ***$p<0.001$, ****$p<0.0001$ by two tailed student's t-test (A, F, and G). Data is representative of ≥3 independent experiments, bars in plots indicate mean ± SEM.

Figure 2

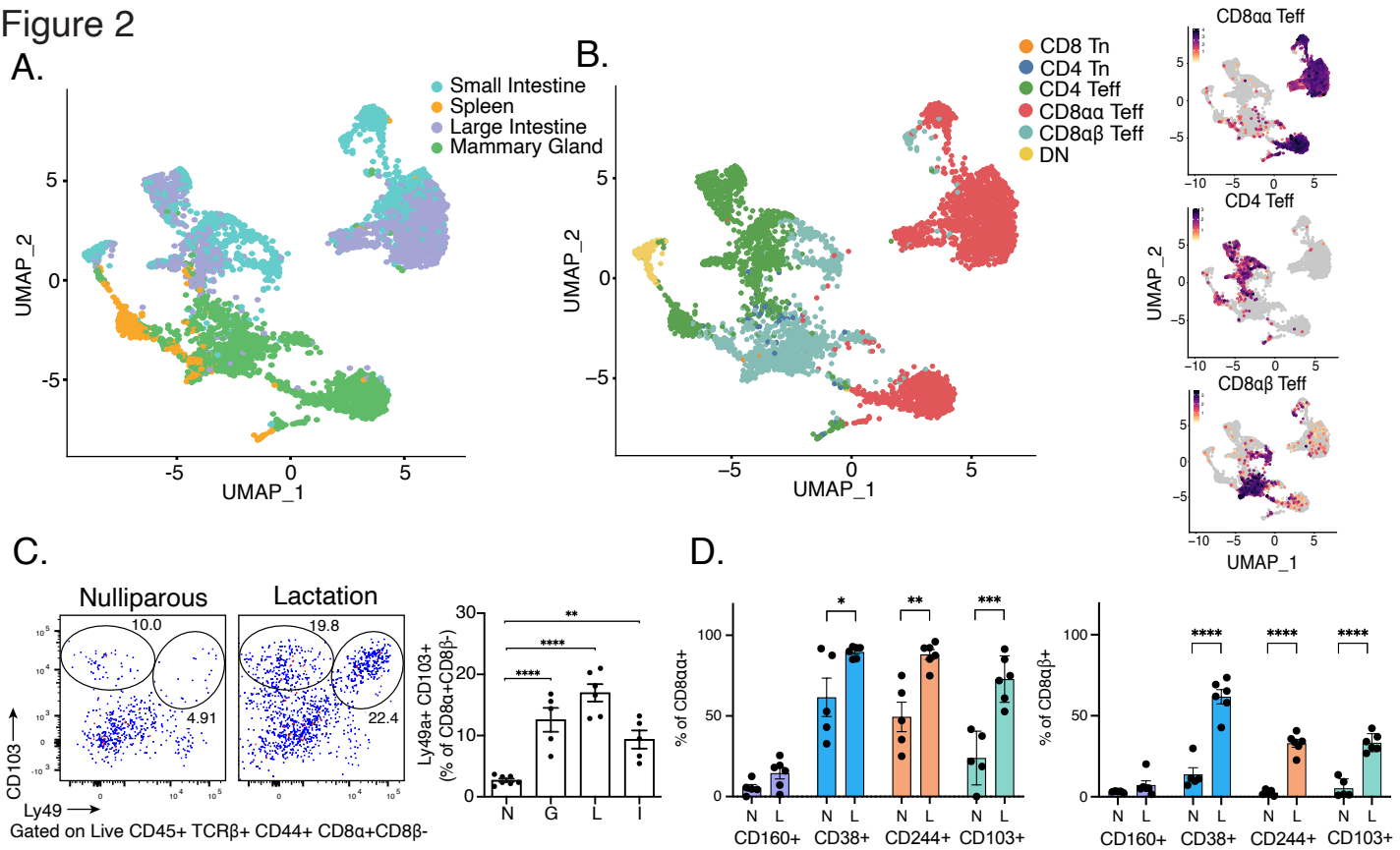
A.
Small Intestine
Spleen
Large Intestine
Mammary Gland
UMAP_2
UMAP_1
B.
CD8 Tn
CD4 Tn
CD4 Teff
CD8αα Teff
CD8αβ Teff
DN
CD8αα Teff
CD4 Teff
CD8αβ Teff
C.
Nulliparous
Lactation
10.0
4.91
19.8
22.4
CD103
Ly49
Gated on Live CD45+ TCRβ+ CD44+ CD8α+CD8β-
Ly49a+ CD103+ (% of CD8α+CD8β-)
N
G
L
I
D.
% of CD8αα+
% of CD8αβ+
CD160+
CD38+
CD244+
CD103+

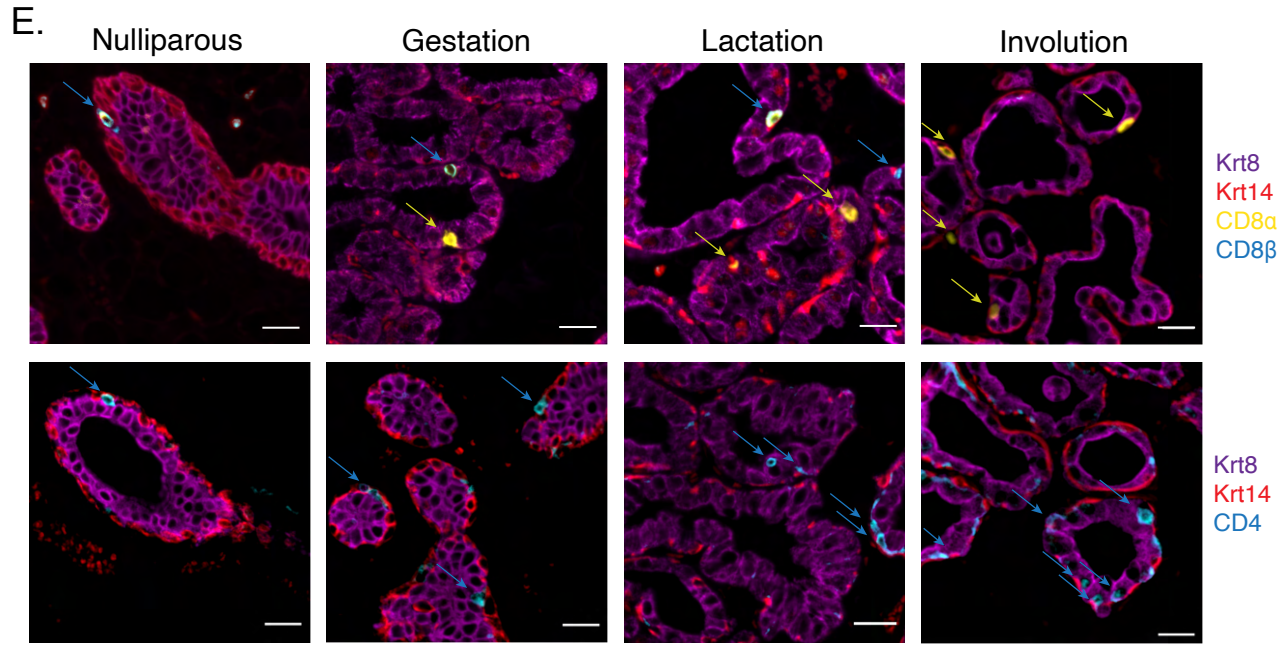
E.
Nulliparous
Gestation
Lactation
Involution
Krt8
Krt14
CD8α
CD8β
Krt8
Krt14
CD4

**Figure 2. Mammary T cells are intraepithelial lymphocytes.**

A) Summary UMAP projections of single cell sequencing performed on T cells from mammary gland, large intestine, spleen and small intestine of lactating mice.

B) UMAP and feature plots showing the transcriptional localization of featured T cell signatures.

C) Representative flow cytometry plots and quantification of CD103+Ly49+CD8αα+ T cells (gated on Live CD45+TCRβ+CD8α+CD8β-) across gestational and lactation stages in the mammary gland. N=nulliparous (n=7), G=gestation day 17 (n=5), L=lactation days 3-5 (n=6) and I=involution,1 day post weaning (n=5).

D) Proportion of CD8αα+ (left) and CD8αβ+ (right) cells that express CD160, CD38, CD244, and CD103 in nulliparous (n=5) and lactation (n=6) mammary glands.

E) Representative immunofluorescence images of the mammary gland at nulliparous, gestation (G17), lactation (L3), and involution. Epithelial cells (Krt8+ luminal cells in magenta and Krt14+ basal cells in red), and T cells, CD8α in yellow, CD8β in cyan (top) and CD4 in cyan (bottom). Scale bar = 20μm.

*$p<0.05$, **$p<0.01$, ***$p<0.001$, ****$p<0.0001$ by two tailed student's t-test (D). Representative of ≥3 independent experiments, bars in plots indicate mean ± SEM.

Figure 3

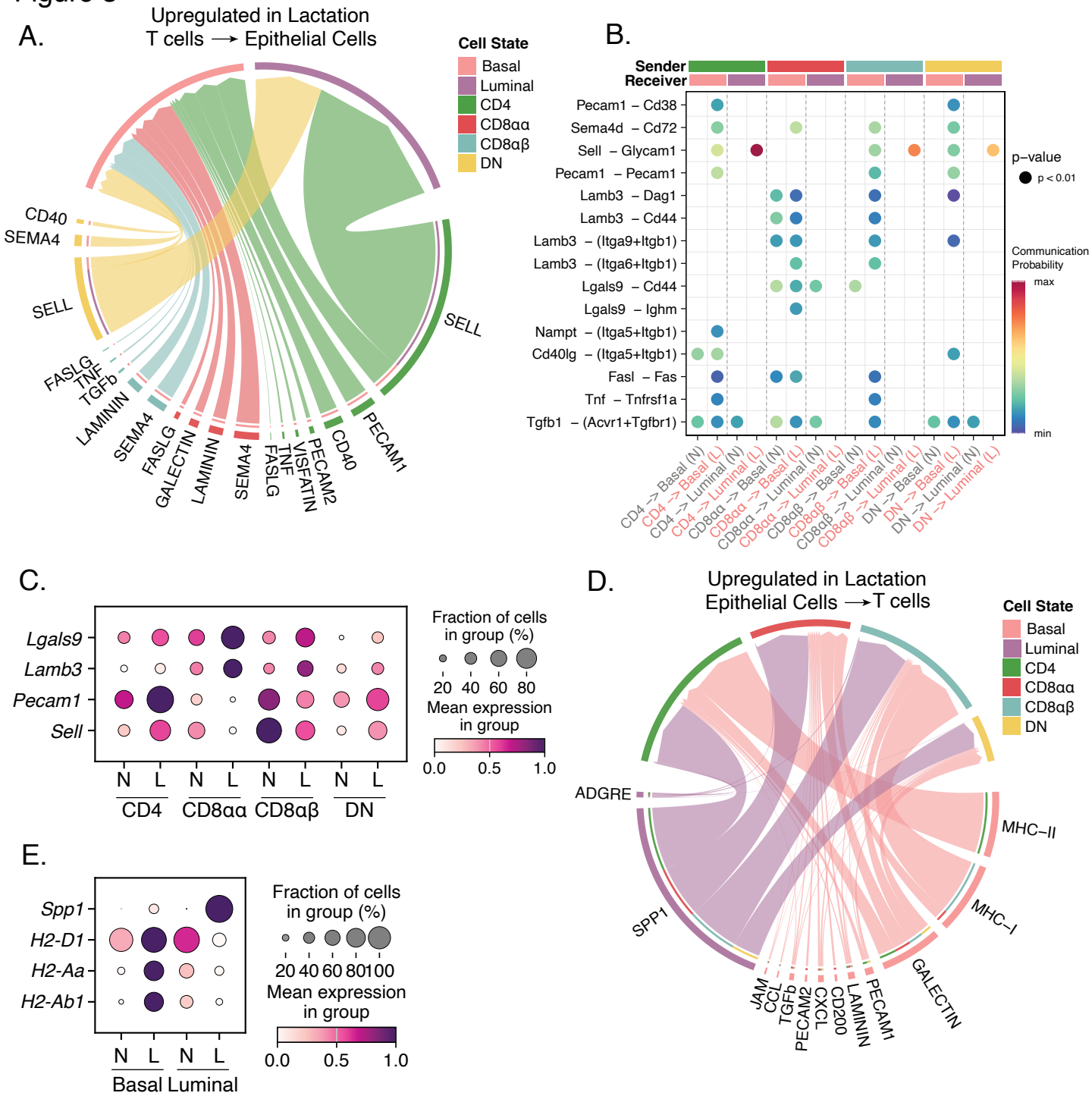
A.
Upregulated in Lactation
T cells → Epithelial Cells
Cell State
Basal
Luminal
CD4
CD8αα
CD8αβ
DN
CD40
SEMA4
SELL
FASLG
TNF
TGFb
LAMININ
SEMA4
FASLG
GALECTIN
LAMININ
SEMA4
FASLG
TNF
VISFATIN
PECAM2
CD40
PECAM1
SELL
B.
Sender
Receiver
Pecam1 – Cd38
Sema4d – Cd72
Sell – Glycam1
Pecam1 – Pecam1
Lamb3 – Dag1
Lamb3 – Cd44
Lamb3 – (Itga9+Itgb1)
Lamb3 – (Itga6+Itgb1)
Lgals9 – Cd44
Lgals9 – Ighm
Nampt – (Itga5+Itgb1)
Cd40lg – (Itga5+Itgb1)
Fasl – Fas
Tnf – Tnfrsf1a
Tgfb1 – (Acvr1+Tgfbr1)
p–value
p < 0.01
Communication Probability
max
min
CD4 -> Basal (N)
CD4 -> Basal (L)
CD4 -> Luminal (N)
CD4 -> Luminal (L)
CD8αα -> Basal (N)
CD8αα -> Basal (L)
CD8αα -> Luminal (N)
CD8αα -> Luminal (L)
CD8αβ -> Basal (N)
CD8αβ -> Basal (L)
CD8αβ -> Luminal (N)
CD8αβ -> Luminal (L)
DN -> Basal (N)
DN -> Basal (L)
DN -> Luminal (N)
DN -> Luminal (L)
C.
Lgals9
Lamb3
Pecam1
Sell
N L N L N L N L
CD4 CD8αα CD8αβ DN
Fraction of cells in group (%)
20 40 60 80
Mean expression in group
0.0 0.5 1.0
D.
Upregulated in Lactation
Epithelial Cells → T cells
Cell State
Basal
Luminal
CD4
CD8αα
CD8αβ
DN
ADGRE
MHC–II
MHC–I
SPP1
GALECTIN
PECAM1
LAMININ
CD200
CXCL
PECAM2
TGFb
CCL
JAM
E.
Spp1
H2-D1
H2-Aa
H2-Ab1
N L N L
Basal Luminal
Fraction of cells in group (%)
20 40 60 80 100
Mean expression in group
0.0 0.5 1.0

**Figure 3. Putative interaction networks between mammary T cells and epithelial cells.**

A, D) Chord diagrams showing potential signaling pathways upregulated in lactation from T cell populations to epithelial cells (A) and from epithelial cells to T cell populations (D). Ligand:receptor pairs as summarized into functionally related signaling pathways. Outer thicker bars represent the cell population that is the source or target of the signaling pathway in the chord diagram. The inner thinner bar color is the target of the signal. The thickness of the edge represents the signaling strength (communication probability) as calculated by CellChat.

B) Dot plot showing the communication probabilities of ligand:receptor pairs upregulated in lactation from T cells to epithelial cells. Heatmap depicts the communication probability of each ligand pair for each cell pair in nulliparous (N) and lactating (L) mammary glands. Sender and receivers are indicated by the color bars on top.

C, E) Dot plot of transcript expression levels in mammary IELs (C) and epithelial cells (E) in nulliparous (N) and lactating (L) mammary glands, depicting the percent of cells expressing and mean expression levels in each cell population.

Figure 4

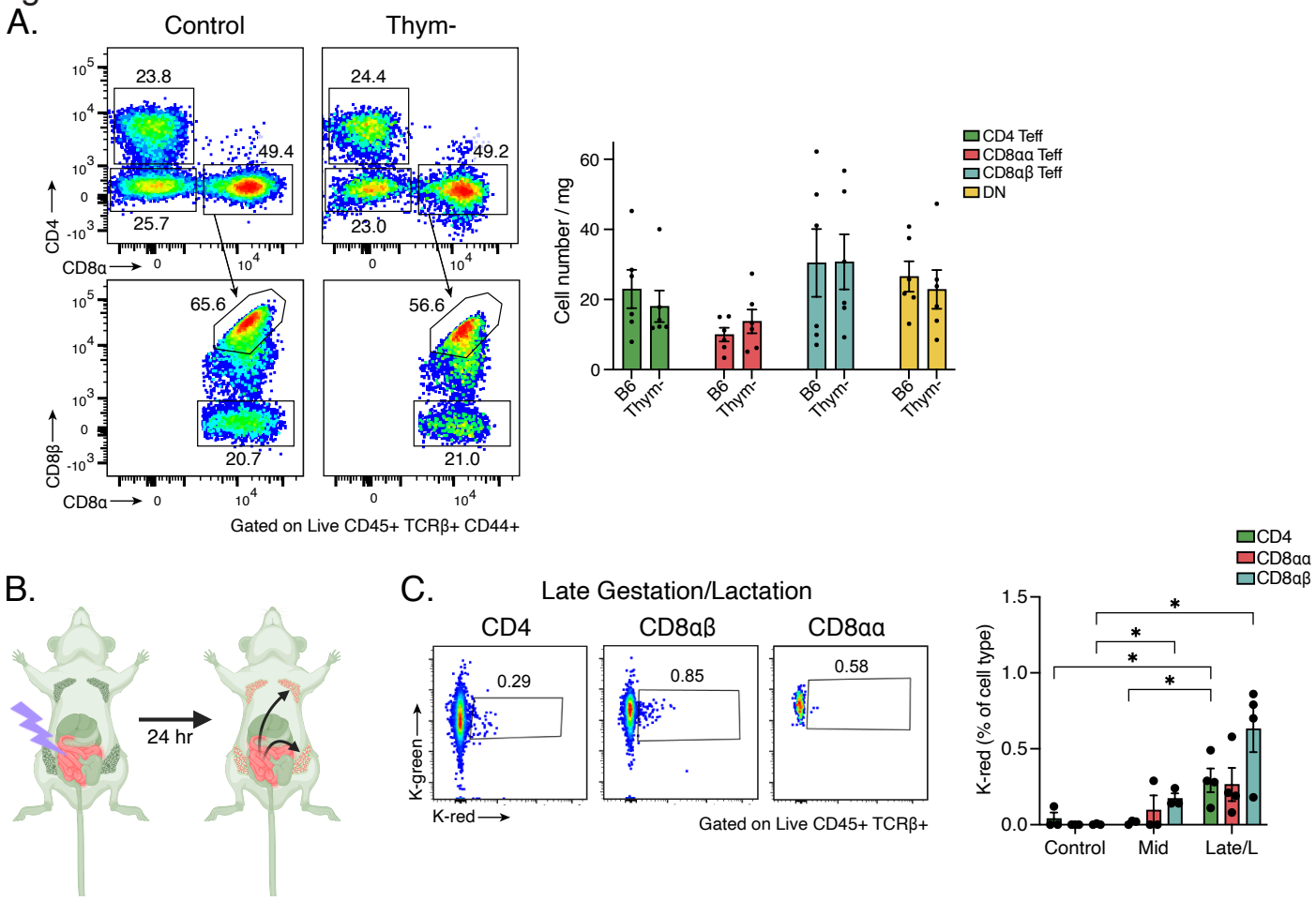
A.
Control
Thym-
23.8
49.4
25.7
24.4
49.2
23.0
CD4
CD8α
65.6
20.7
56.6
21.0
CD8β
Gated on Live CD45+ TCRβ+ CD44+
CD4 Teff
CD8αα Teff
CD8αβ Teff
DN
Cell number / mg
B6
Thym-
B.
24 hr
C.
Late Gestation/Lactation
CD4
CD8αβ
CD8αα
0.29
0.85
0.58
K-green
K-red
Gated on Live CD45+ TCRβ+
CD4
CD8αα
CD8αβ
K-red (% of cell type)
Control
Mid
Late/L

**Figure 4. Intestinal T cells migrate to the mammary gland during late gestation and lactation.**

A) Representative flow cytometry plots and quantification of CD4 Teff, CD8αα+ Teff , CD8αβ+ Teff and DN cell populations in control B6 (n=6) and thymectomized (n=6) lactating mice. Teff populations were determined as CD4 Teff: CD4+CD44+CD62L-. CD8αα Teff: CD8α+CD8β-CD44+CD62L-. CD8αβ Teff: CD8α+CD8β+CD44+CD62L-. DN: TCRβ+CD4-CD8α-.

B) Experimental design for Kaede experiments: intestines of Kaede+ mice were photoconverted from green to red by illumination with UV light after laparotomy in mid-late pregnancy and early lactation, and migration of red cells to the mammary gland examined after 24 hours .

C) Representative flow cytometry plots and quantification of Kaede red cells within T cell populations (gated on TCRβ+ followed by either CD4+ or CD8β+ or CD8α+ CD8β-) in the mammary gland of mice 24 hours post-photoconversion of the intestine. Controls are non-photoconverted mice (n=3), mid being mice photoconverted on gestation day 10 and analyzed on gestation day 11 (n=3) and late/L representing mice both photoconverted on gestation day 16 and analyzed on gestation day 17 and mice photoconverted on lactation day 1 and analyzed on lactation day 2 (n=4).

* $p<0.05$ by two tailed student's t-test (C). Data representative of ≥3 independent experiments, bars in plots indicate mean ± SEM.

Figure 5

A.

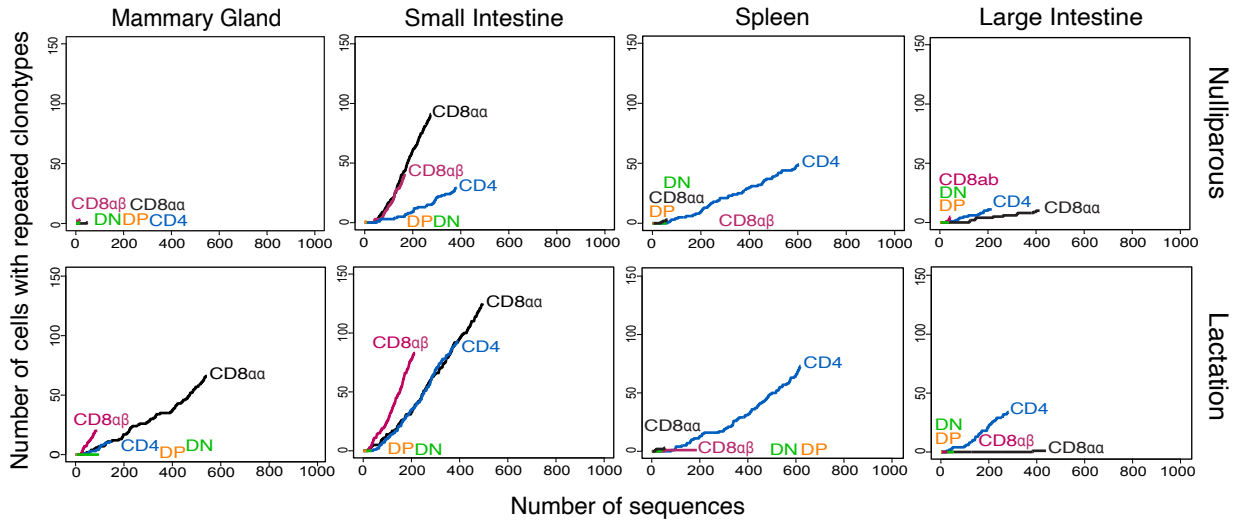


B.

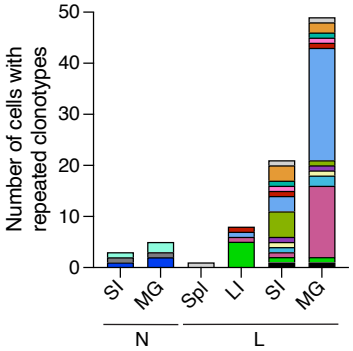


C.

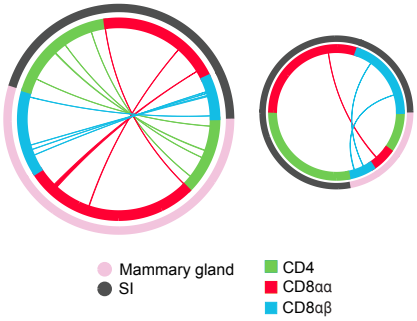


D.

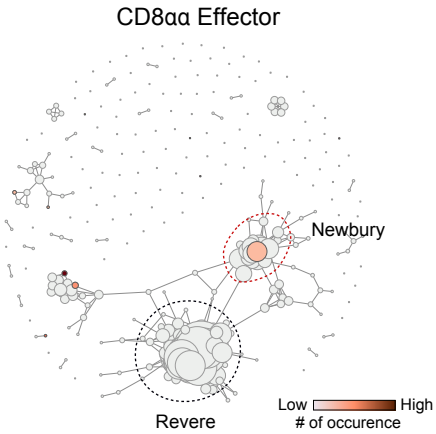


E.

F.

| | Mouse | Tissue | Cell type | Va | Ja | CDR3α | Vb | Jb | CDR3β |
|---|---|---|---|---|---|---|---|---|---|
| Newbury | m1 | SI IEL | CD8aa | TRAV12-2 | TRAJ22 | CALSASSGSWQLIF | TRBV13-1 | TRBJ2-7 | CASSDFGGFHEQYF |
| | m2 | SI IEL | CD8aa | TRAV12-3 | TRAJ22 | CALTPASSGSWQLIF | TRBV13-1 | TRBJ2-7 | CASSDTGGEYEQYF |
| | m2 | SI IEL | CD8aa | TRAV12-3 | TRAJ22 | CALSPASSGSWQLIF | TRBV13-1 | TRBJ2-5 | CASSDADREDTQYF |
| | m3 | Lact MG | CD8aa | TRAV12-3 | TRAJ22 | CALTPASSGSWQLIF | TRBV3 | TRBJ2-4 | CASSPTASQNTLYF |
| | m3 | Lact MG | CD8aa | TRAV12-2 | TRAJ22 | CALSASSGSWQLIF | TRBV13-2 | TRBJ2-3 | CARTGTEAETLYF |
| | m3 | Lact MG | DN | TRAV12-2 | TRAJ22 | CALSASSGSWQLIF | TRBV13-1 | TRBJ2-7 | CASSEGLSSYEQYF |
| Revere | m2 | SI IEL | CD8aa | TRAV6-2 | TRAJ22 | CVLGASSGSWQLIF | TRBV3 | TRBJ1-4 | CASSPGTISNERLFF |
| | m2 | SI IEL | CD8aa | TRAV16N | TRAJ22 | CAMRASSGSWQLIF | TRBV14 | TRBJ1-4 | CASSPGTISNERLFF |
| | m1 | SI IEL | CD8aa | TRAV7-6 | TRAJ22 | CAVASSGSWQLIF | TRBV12-1 | TRBJ1-4 | CASSSGTISNERLFF |
| | m4 | Lact MG | CD8aa | TRAV6D-5 | TRAJ22 | CVLSSGSWQLIF | TRBV12-1 | TRBJ1-4 | CASSPGTISNERLFF |
| | m3 | Lact MG | CD8aa | TRAV6-3 | TRAJ22 | CAMRALSSGSWQLIF | TRBV13-1 | TRBJ1-4 | CASSPGTISNERLFF |
| | m4 | Lact MG | DN | TRAV7-2 | TRAJ22 | CAASISGSWQLIF | TRBV3 | TRBJ1-4 | CASSSGTISNERLFF |

G.

| Tissue | CD8αα+ counts | Revere + Newbury counts | Percentage |
|---|---|---|---|
| SI | 6577 | 264 | 4.01 |
| Peritoneal cavity | 28 | 1 | 3.57 |
| Colon | 2324 | 3 | 0.13 |
| Mammary gland | 857 | 4 | 0.47 |
| Blood | 45 | 0 | 0.00 |
| Bone marrow | 239 | 0 | 0.00 |
| Liver | 205 | 0 | 0.00 |
| LN | 54 | 0 | 0.00 |
| Lung | 108 | 0 | 0.00 |
| Salivary gland | 45 | 0 | 0.00 |
| Spleen | 158 | 0 | 0.00 |
| Tumor | 80 | 0 | 0.00 |
| Uterus | 258 | 0 | 0.00 |
| All other tissues | 3544 | 4 | 0.11 |

**Figure 5. Mammary T cells share peculiar TCR repertoires with small intestinal T cells.**

A) Rarefaction analysis from TCR sequencing of T cell types between nulliparous and lactating mice in the mammary gland, small intestine, spleen and large intestine.

B) Quantification of the number of cells with repeated clonotypes between organs in a nulliparous and lactating mouse. Each color representing a unique clonotype.

C) Chord diagrams in lactating (L3) and nulliparous mice representing clonotype sharing in different T cell populations (inner ring) between the small intestine and mammary gland (outer ring). Each line represents a TCR clonotype.

D) Distance matrix between αβTCR clonotypes in intestinal IELs. Red circle denotes "Newbury TCR" and black circle denotes "Revere TCR".

E) CDR3 sequence of Revere and Newbury TCRs.

F) Table representing instances of Revere and Newbury TCRs in CD8αα+ T cells in mammary gland and small intestine across different mice.

G) Counts of Revere and Newbury TCRs in CD8αα+ T cells across multiple tissues.

Data representative of ≥3 independent experiments.

Figure 6

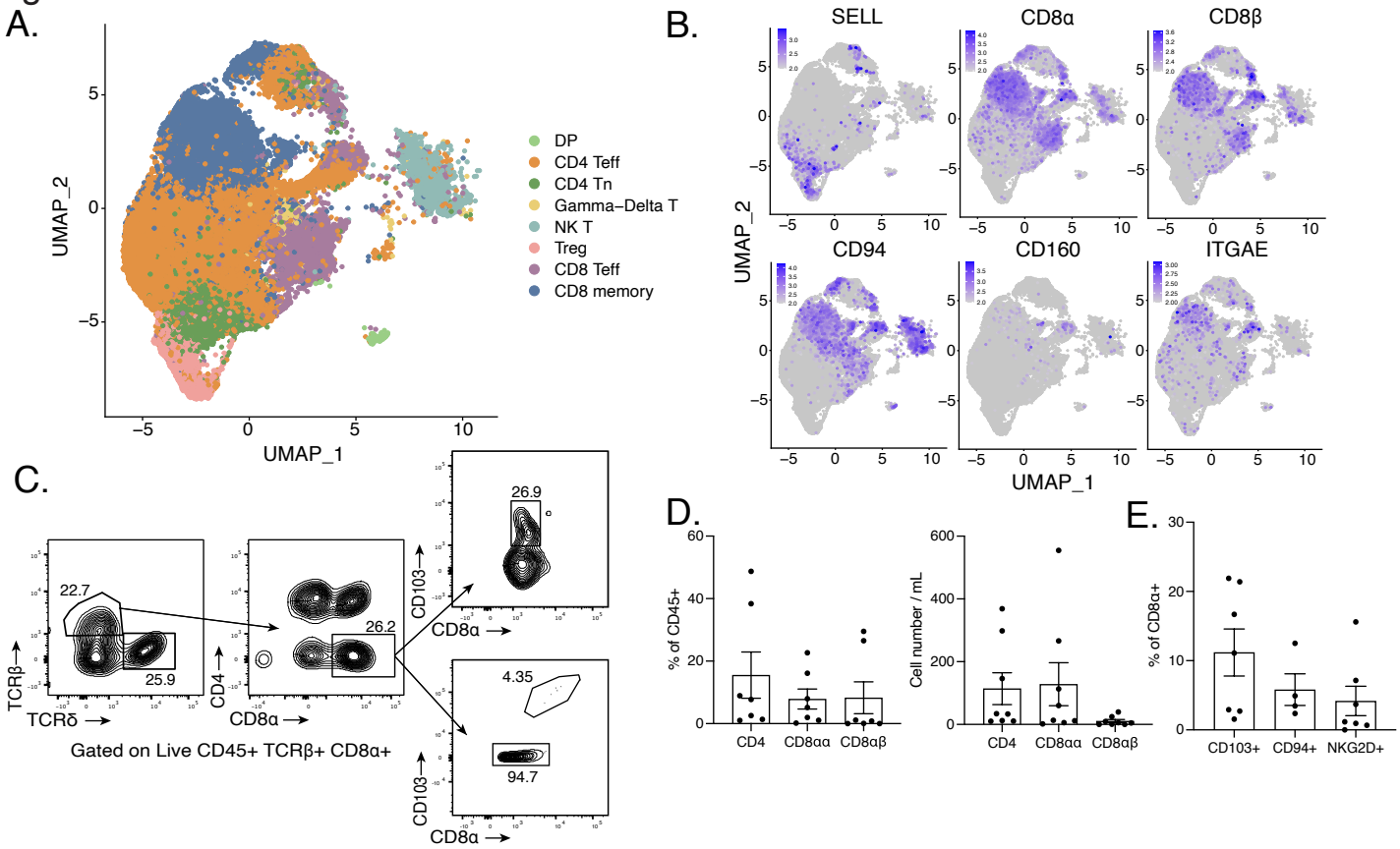
A.
UMAP_2
UMAP_1
DP
CD4 Teff
CD4 Tn
Gamma−Delta T
NK T
Treg
CD8 Teff
CD8 memory
B.
SELL
CD8α
CD8β
CD94
CD160
ITGAE
UMAP_2
UMAP_1
C.
22.7
25.9
TCRβ
TCRδ
26.2
CD4
CD8α
26.9
CD103
CD8α
4.35
94.7
CD103
CD8α
Gated on Live CD45+ TCRβ+ CD8α+
D.
% of CD45+
CD4
CD8αα
CD8αβ
Cell number / mL
CD4
CD8αα
CD8αβ
E.
% of CD8α+
CD103+
CD94+
NKG2D+

**Figure 6. Mammary IEL-like cells are found in human breast and milk.**

A) UMAP projection of mammary immunocytes from human breast tissue (sourced from Kumar et al).

B) Feature plots of selected genes projected on UMAP from (A).

C) Representative flow cytometry gating of CD8α+ CD103+ T cells and CD8αα+ IEL-like cells in human milk samples.

D) Quantification of CD4+, CD8αα+ and CD8αβ+ cells as percent of CD45+ cells (left) (n=7) and cell number normalized to volume (right) (n=8) in human milk samples.

E) Proportion of human CD8αα IEL- like cells that express markers CD103 (n=7), CD94 (n=4), and NKG2D (n=7) in human milk samples.

Data represents ≥7 independent milk samples/experiments, bars in plots indicate mean ± SEM. Single cell sequencing from Kumar et al.

Figure 7

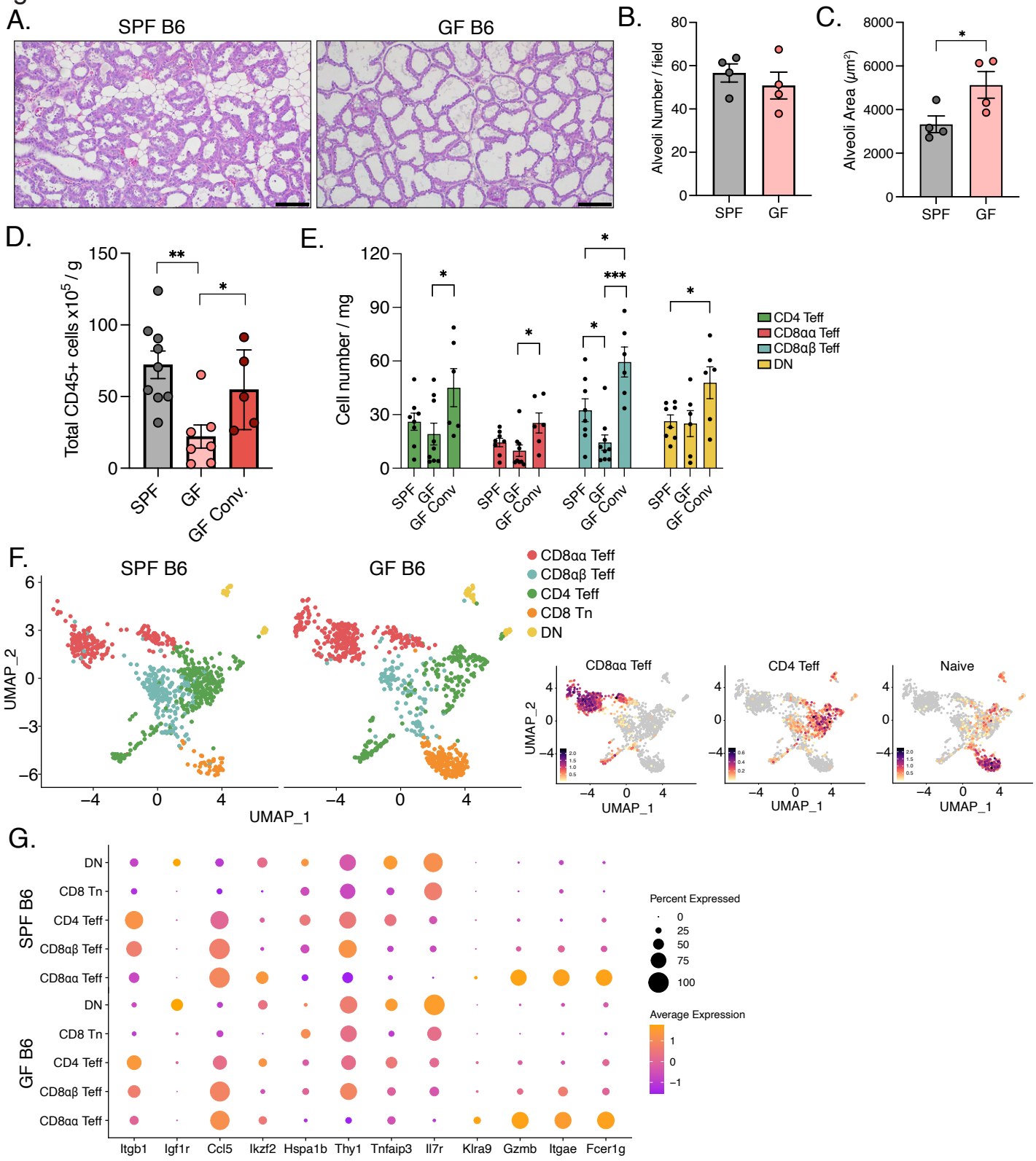
A.
SPF B6
GF B6
B.
Alveoli Number / field
SPF
GF
C.
Alveoli Area (μm²)
SPF
GF
D.
Total CD45+ cells x10⁵ / g
SPF
GF
GF Conv.
E.
Cell number / mg
SPF
GF
GF Conv
CD4 Teff
CD8αα Teff
CD8αβ Teff
DN
F.
SPF B6
GF B6
CD8αα Teff
CD8αβ Teff
CD4 Teff
CD8 Tn
DN
UMAP_1
UMAP_2
CD8αα Teff
CD4 Teff
Naive
G.
SPF B6
GF B6
DN
CD8 Tn
CD4 Teff
CD8αβ Teff
CD8αα Teff
Itgb1
Igf1r
Ccl5
Ikzf2
Hspa1b
Thy1
Tnfaip3
Il7r
Klra9
Gzmb
Itgae
Fcer1g
Percent Expressed
Average Expression

**Figure 7. T cell expansion in the lactating mammary gland is partially dependent on microbes.**

A) Representative hematoxylin and eosin staining of lactating mammary gland of specific pathogen free (SPF) and germfree (GF) mice. Scale bar = 100μm.

B, C) Quantification of the average number (B) and average area ($\mu m^2$) (C) of alveoli per 20x image fields (five images per mouse of size 900μm x 500μm) of SPF and GF mammary glands (n=4).

D) Quantification of the total number of CD45+ cells normalized to mammary gland weight in SPF (n=9), GF (n=7) and GF conventionalized mice (n=5).

E) Quantification of total cell numbers normalized to mammary gland weight, of specified T cell populations in SPF (n=8), GF (n=9, n=6 for DN) and GF conventionalized (n=6) mice by flow cytometry. Teff populations were determined as CD4 Teff: CD4+CD44+CD62L-. CD8αα Teff: CD8α+CD8β-CD44+CD62L-. CD8αβ Teff: CD8α+CD8β+CD44+CD62L-. DN: TCRβ+CD4-CD8α-.

F) UMAP projection of mammary T cells from lactating SPF and GF mice with feature plots of naïve and effector T cell gene signatures.

G) Dot plot of differentially expressed genes in mammary T cell populations between lactating SPF and GF mice from (F).

*$p<0.05$, **$p<0.01$ ***$p<0.001$ by student's t-test. Data representative of ≥3 independent experiments, bars in plots indicate mean ± SEM.